College of Engineering

Probing elastic modulus and depth of bottom-supported inclusions in model tissues using piezoelectric cantilevers

Hakki Yegingil
Department of Materials Science and Engineering, Drexel University, Philadelphia, Pennsylvania 19104, USA

Wan Y. Shih
School of Biomedical Engineering, Science and Health Systems, Drexel University, Philadelphia, Pennsylvania 19104, USA

Wei-Heng Shih
Department of Materials Science and Engineering, Drexel University, Philadelphia, Pennsylvania 19104, USA

(Received 2 April 2007; accepted 10 September 2007; published online 2 November 2007)

We have experimentally investigated the depth sensitivity limit of a piezoelectric cantilever tissue elastic modulus sensor and simultaneously determined the elastic modulus and the depth of a tumor directly. Using model tissues consisting of bottom-supported modeling clay inclusions of various depths in a gelatin matrix, we empirically determined that the depth sensitivity limit of a piezoelectric cantilever sensor was twice the linear dimension of the indentation area (or the cantilever width). Knowing the depth sensitivity limit of the individual cantilever sensor as input and treating a model tissue that has the gelatin matrix on top and the modeling clay inclusion at the bottom as two springs in series, we showed that the elastic moduli and depths of the hard inclusions could be simultaneously determined with the elastic modulus profiles measured by two cantilevers with different widths as input. © *2007 American Institute of Physics*. [DOI: 10.1063/1.2793502]

I. INTRODUCTION

The elastic modulus of abnormal tissues such as breast tumors differs from surrounding normal tissues.[1] Often the difference can be several folds.[2] This difference provided the motivation to seek measurement technologies that can assess tumors or regions of tissues of abnormal stiffness mechanically. It would be desirable to be able to assess tissue abnormality *in vivo*. Typical soft-tissue mechanical property testers[3–10] require specimens to be cut to a certain shape to fit in the tester and thus are unfit for *in vivo* measurements. To measure the elastic properties of soft tissues *in vivo*, one typically uses an indenter to depress the tissue and measures the depth of the indentation with a linear variable differential transducer[11] or an ultrasound transducer,[12–14] or using magnetic resonance imaging techniques.[15] With these techniques, computations using inversion techniques are required to estimate the size, elastic modulus, and depth of the tumor.[16–18] It will be beneficial to develop measurement techniques that can experimentally determine tumor elastic modulus, depth, and size noninvasively without relying on simulations or inversion techniques.

Recently, we have developed a piezoelectric cantilever sensor that has a driving piezoelectric layer for force application and a sensing piezoelectric layer for displacement determination for all-electrical palpationlike elastic modulus/shear modulus measurement,[19–22] offering potential for *in vivo* elastic and shear modulus imaging applications. A schematic of a piezoelectric cantilever in indentation geometry for elastic modulus measurement is shown in Fig. 1. For shear modulus measurements, the cantilever would rotate 90° to be perpendicular to the sample surface.[19,22] A piezoelectric cantilever has been demonstrated to be capable of imaging the elastic modulus differences between the tumor region and the surrounding tissues in excised breast tissues[20] and between a hard inclusion and the soft matrix in model tissues.[21,22] Using the width at half the peak elastic/shear modulus, the lateral size of the tumor or hard inclusion could be estimated. What remains unclear is the depth sensitivity limit under the indentation (or palpationlike) geometry of the piezoelectric cantilever. Preliminary results indicated that tumors or hard inclusions too deep underneath the surface were undetectable by a piezoelectric cantilever.[21] This is understandable as the palpationlike or indentation measurement is a technique that only affects a limited region beneath the surface. If one can measure the depth sensitivity limit of a piezoelectric sensor, it will be possible to use piezoelectric cantilevers to measure the depth and the elastic/shear modulus of a tumor without relying on inversion simulations.

The purpose of this study is to experimentally investigate the depth sensitivity limit of a piezoelectric cantilever elastic modulus sensor and to explore the use of two piezoelectric cantilevers with different widths to simultaneously determine the elastic modulus and the depth of a tumor on model tissues consisting of bottom-supported modeling clay inclusions in a gelatin matrix. In the following, all inclusions are meant to be bottom-supported inclusions. The present modeling clay inclusions which mimic breast tumors had elastic moduli in the range of 40–150 kPa as similar to those of breast tumors.[3] The gelatin matrix which mimics the surrounding breast tissue had an elastic modulus of a few kilopascal as analogous to those of normal breast tissues.[3] In

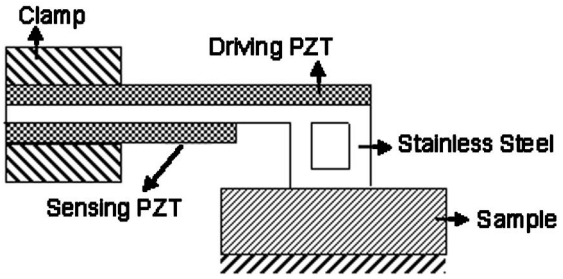

FIG. 1. A schematic of an all-electrical piezoelectric cantilever performing a compression test. The cantilever has a top PZT layer for driving, a bottom PZT layer for sensing, and a stainless steel tip that has a square contact area with the sample.

what follows, all experiments were done in the indentation geometry for elastic modulus measurements. It should be noted that the methodology discussed in this study for elastic modulus measurements also applies to shear modulus measurements. The rest of the paper is organized as follows. Section 2 describes the fabrication and characterization of the piezoelectric cantilevers, the all-electrical indentation (palpationlike) tissue elastic modulus measurements, the methodology of simultaneous determination of tumor depth and tumor elastic modulus using two cantilevers, and the fabrication of model tissues. Section 3 gives the results and discussions.

II. EXPERIMENT PROCEDURE AND METHODS

A. Cantilever fabrication and characterization

Three piezoelectric cantilevers were used in this study. Cantilever A was 3.8±0.2 mm wide, cantilever B was 6.1±0.2 mm wide, and cantilever C was 8.6±0.2 mm wide as listed in Table I. All cantilevers had two 127 μm thick lead zirconate titanate (PZT) layers (T105-H4E-602, Piezo Systems Inc., Cambridge, MA) bonded to a 50 μm thick stainless steel layer (Alfa Aesar, Ward Hill, MA), one on the top side of the stainless steel for driving and the other on the bottom side of the stainless steel for sensing as schematically shown in Fig. 1, using a nonconductive epoxy (Henkel Loctite Corporation, Industry, CA), followed by curing at room temperature for one day and sanding of the edges for uniformity. The driving PZT layers were 22±0.2, 24±0.2, and 25±0.2 mm long and sensing PZT layers were 11±0.2, 12±0.2, and 11±0.2 mm long for cantilevers A, B, and C, respectively (see Table I). The stainless steel tip was fashioned into a square loop at the free end with each side of the square equal to the width of the cantilever to facilitate both compression and shear measurements using one single cantilever. The cantilevers were clamped with a fixture made of 7.5 mm thick acrylic (McMaster-Carr, New Brunswick, NJ). The PZT layers have a piezoelectric coefficient, $d_{31}=-320$ pC/N. Young's modulus of the stainless steel and that of the PZT layers were 200 and 62 GPa, respectively. The capacitance and the loss factor of a PZT layer were measured using an Agilent 4294A Impedance Analyzer (Agilent, Palo Alto, CA).

TABLE I. Dimensions of cantilevers A, B, and C.

Cantilever	Length (mm)		Width (mm)	Probe area (mm^2)
	Driving PZT	Sensing PZT		
A	22±0.2	11±0.2	3.8±0.2	14±1
B	24±0.2	12±0.2	6.1±0.2	37±3
C	25±0.2	11±0.2	8.6±0.2	74±4

In an indentation measurement, as the square stainless steel tip cross section was much smaller than the sample surface, it was the square stainless steel tip cross section that defined the area of indentation. The contact areas were 14±1, 37±3, and 74±4 mm^2, the square of the widths of cantilevers A, B, and C, respectively (see Table I).

For cantilever tip displacement measurements, Keyence model LC-2450 (Keyence Corporation, Osaka, Japan) laser displacement meter with a 0.5 μm resolution was used. The effective spring constants K of cantilevers A, B, and C were 143, 187, and 215 N/m as determined using the earlier published procedure.[21,22] A dc power supply, HP E3631A, (Hewlett-Packard Company, Palo Alto, CA), was used as the programmable dc voltage source. The measurements were conducted on a Newport optical table (RS1000, Newport Corporation, Irvine, CA) to minimize low-frequency background vibrations. The applied voltage across the driving PZT layer and the induced voltage across the sensing PZT layer were recorded on an Agilent Infiniium S4832D digital oscilloscope (Agilent, Palo Alto, CA). The dc power source and the oscilloscope were connected to a personal computer (PC). All voltage measurements, real-time elastic modulus computations, and data acquisitions were controlled from a PC by LABVIEW (National Instrument, Austin, TX) programing.

B. Induced voltage measurements

When a dc voltage is applied across the driving PZT layer, a measurable piezoelectric voltage is induced across the sensing PZT layer.[21,22] As an example, the induced voltage versus time of cantilever A at various applied voltages is shown in Fig. 2(a). As can be seen, the induced voltage increased sharply initially to a maximum then decayed exponentially with time due to the finite resistance of the PZT. In Fig. 2(b), we show the peak induced piezoelectric voltage versus the cantilever tip displacement. Figure 2(b) shows that the peak induced voltage was proportional to the cantilever tip displacement,[21,22] and thus can be used to represent the cantilever tip displacement. With the spring constant of the cantilever, $K=143$ N/m, the cantilever tip displacement shown in the x axis of Fig. 2(b) can also be translated into a force, $F=Kd$, exerted on the cantilever tip, where d represents the cantilever tip displacement. The equivalent force associated with a tip displacement d is labeled on the top x axis of Fig. 2(b). Figure 2(b) clearly illustrates that the peak induced piezoelectric voltage can be used to monitor the cantilever tip displacement as well as the equivalent force at the cantilever tip. This is the basis of the cantilever's all-electrical elastic modulus measurements. In what follows, we will refer to the peak induced piezoelectric voltage simply as the induced voltage V_{in}.

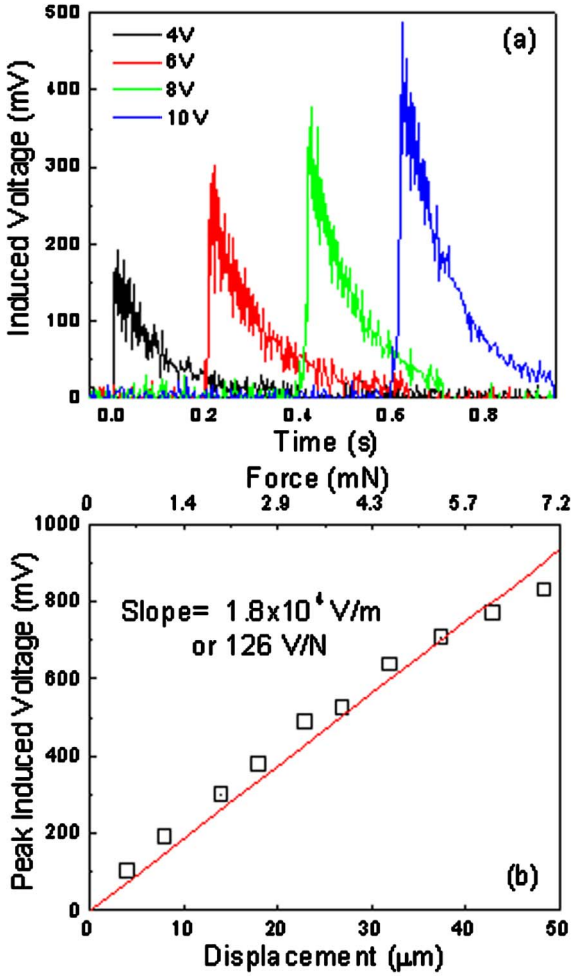

FIG. 2. (Color online) (a) Induced piezoelectric voltage vs time at the sensing PZT when a voltage was applied to the driving PZT layer and (b) peak induced voltage vs tip displacement (force on top) of cantilever A.

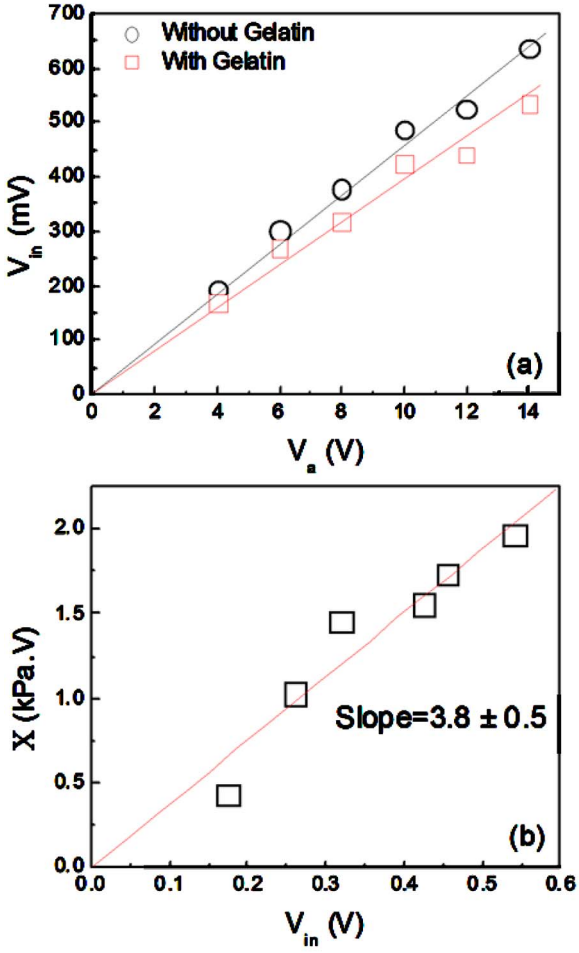

FIG. 3. (Color online) (a) V_{in} vs V_a of cantilever A without (open circles) and with (open squares) the gelatin sample and (b) X vs V_{in} where X is as defined in the text. The slope of X vs V_{in} gave the elastic modulus of the gelatin sample.

C. All-electrical indentation elastic modulus measurements

Since the induced voltage across the sensing electrode is linear to the displacement and the force at the cantilever tip, one can calibrate the corresponding force and displacement with the induced voltage and express the displacement, force, and elastic moduli in terms of the induced voltage.[21,22] First, the induced voltages of the cantilevers at various applied voltages V_a were measured without and with a sample underneath the cantilever tip. As an example, we plot V_{in} vs V_a of cantilever A without and with a gelatin sample (G7-500, Fisher Scientific, Fair Lawn, NJ) in Fig. 3(a). The concentration of the gelatin was 0.07 g/ml prepared by mixing 19.25 g of gelatin in 275 ml of water at 80 °C on a hot plate for 5 min, cooled at 5 °C for 1 h to solidify, and then equilibrated at room temperature for 1 h prior to measurements. The gelatin obtained as described above was the gelatin matrix for the model tissues we used in this study. With $V_{in,0}$ denoting the induced voltage without a sample under the indentation geometry, the elastic modulus E of the gelatin sample could be deduced as[21,22]

$$E = \frac{X}{V_{in}}, \tag{1}$$

where

$$X = \frac{1}{2}\left(\frac{\pi}{A}\right)^{1/2}(1-\nu^2)K(V_{in,0}-V_{in}), \tag{2}$$

with ν=0.5 being Poisson's ratio of the gelatin sample,[21,22] A the contact area of the cantilever stainless steel tip, and K the effective spring constant of the cantilever. Therefore, once the induced voltages without and with the sample were measured, the elastic modulus of the sample can be readily obtained from the slope of X vs V_{in}. Note that in the present study, X vs V_{in} was linear with little hysteresis between the up sweep and down sweep. The reason for this lack of hysteresis is that the strains in these studies are very small, less than 0.1%. If larger strains are involved, generally, X vs V_{in} may not be linear and the elastic modulus should be deduced from the down sweep near the maximum V_{in}.[23] Measurement of V_{in}, computation of X, plotting of X vs V_{in}, and real-time extraction of the elastic modulus from the slope of X vs V_{in} were all carried out through LABVIEW. Note that Eqs. (1) and (2) are for a circular indentation area. Approximating the current square contact area as circular was justified as the error of using a circular indenter formula for the present square contact area was only 1.2%,[23] which was smaller than the present experimental error. From Fig. 3(b), one could deduce the elastic modulus of the gelatin matrix from the

TABLE II. The summary of the known depth and modulus of the inclusions used in models I and II.

	Model I		Model II	
Inclusion No.	Known depth (mm)	Known elastic modulus (kPa)	Known depth (mm)	Known elastic modulus (kPa)
1	1±0.3	145±10	2±0.3	145±10
2	3±0.3	145±10	2±0.3	92±9
3	5.5±0.3	145±10	2±0.3	54±12
4	6.5±0.3	145±10	4±0.3	145±10
5	9±0.3	145±10	4±0.3	92±9
6	11±0.3	145±10	4±0.3	54±12
7	13±0.3	145±10	6±0.3	145±10
8	15±0.3	145±10	6±0.3	92±9
9	16.5±0.3	145±10	6±0.3	54±12

slope as 3.8±0.5 kPa, which was consistent with the elastic modulus of gelatin of this concentration made with the above procedure. In what follows, all elastic modulus measurements were carried out using the indentation geometry, and the elastic modulus was deduced, as illustrated in Figs. 3(a) and 3(b) automatically through LABVIEW.

D. Depth sensitivity measurements

To examine the depth sensitivity limit of the cantilevers, a model consisting of a gelatin matrix (G7-500, Fisher Scientific, Fair Lawn, NJ) with red modeling clay (Modeling Clay, Crayola, Easton, PA) inclusions buried at various depths underneath the surface was prepared. Indentation tests were carried out at the center of the gelatin surface above the center of each inclusion to determine the effective elastic modulus of the model tissue which contained the gelatin on the top and the modeling clay inclusion at the bottom. Conceivably, as the inclusions became too deep below the surface, the effective modulus would converge to that of the gelatin matrix. The depth sensitivity limit of a cantilever was therefore determined as the depth of the inclusion (defined as the distance from the gelatin surface to the top surface of the inclusion) beyond which the measured elastic modulus of the model tissue was indistinguishable from that of the gelatin matrix. Nine inclusions, each with a 16×16 mm^2 top surface but a different height, were glued to the bottom of a container with 24 mm height (model I). The gelatin matrix had a concentration of 0.07 g/ml as prepared by mixing 19.25 g of gelatin in 275 ml of water at 80 °C on a hot plate for 5 min, poured over the model clay inclusions, and then cooled at 5 °C for 1 h to solidify. The sample was allowed to equilibrate at room temperature for 1 h prior to the measurements. The total height of the gelatin of model I was 24±0.3 mm. The depths of the nine inclusions in model I are listed in Table II.

E. Empirical determination of depth and elastic modulus of inclusions

To illustrate the empirical determination of the inclusion elastic modulus and inclusion depth, we embedded three different types of modeling clay inclusions of various depths (model II). Each type of modeling clay had a different stiffness. The elastic moduli of the three different types of modeling clay were independently measured using the procedures described in Sec. II C. The green modeling clay (Play-Doh, Hasbro Ltd., Newport, UK) was softer with an elastic modulus of 54±12 kPa. The blue modeling clay (Model Magic, Crayola, Easton, PA) was intermediate with an elastic modulus of 92±9 kPa, and the red modeling clay (Modeling Clay, Crayola, Easton, PA), which was also used in model I, was stiffer with an elastic modulus of 145±10 kPa. The gelatin matrix used had the same concentration and preparation procedure as described above. All the inclusions in model II were also bottom supported. The total height of the gelatin in model II was 20±0.3 mm. The "known" depths and elastic moduli of the nine inclusions in model II are also listed in Table II.

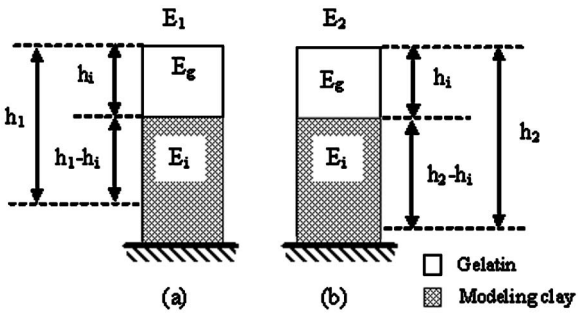

FIG. 4. A schematic illustrating that for the inclusion of depth h_i, the measured elastic modulus was (a) E_1 by cantilever 1 with a depth sensitivity h_1 and (b) E_2 by cantilever 2 with a depth sensitivity h_2.

After the depth sensitivity limit of each cantilever was determined, as described in Sec. II D, it is possible to deduce both the elastic modulus of the inclusion E_i and the inclusion depth h_i (defined as the distance from the gelatin surface to the top surface of the inclusion) from the measurements of two cantilevers of different widths (cantilever 1 and cantilever 2). With the depth sensitivity limit of cantilever 1 and that of cantilever 2 designated as h_1 and h_2 and the effective modulus of the model tissue measured by cantilever 1 and cantilever 2 at the gelatin surface above the center of inclusion as E_1 and E_2—and assuming the gelatin and the inclusion as two springs in series—the effective elastic moduli, E_1 and E_2, can then be expressed as

$$\frac{h_1}{E_1} = \frac{h_i}{E_g} + \frac{(h_1 - h_i)}{E_i}, \tag{3}$$

$$\frac{h_2}{E_2} = \frac{h_i}{E_g} + \frac{(h_2 - h_i)}{E_i}. \tag{4}$$

A schematic of the "two-spring model" for the model tissue with an inclusion of elastic modulus E_i at a depth of h_i is shown in Fig. 4(a) the measurement of E_1 using cantilever 1 that has a depth sensitivity, h_1, and (b) the measurement of E_2 using cantilever 2 that has a depth sensitivity, h_2. As can be seen, there are two unknowns, h_i and E_i, in Eqs. (3) and (4). All other quantities are measurable. Therefore, the two unknowns, h_i and E_i, can be deduced by solving Eqs. (3) and (4) simultaneously using the input from measurements on the same model using two different cantilevers. Note that the implicit assumption of Eqs. (3) and (4) is that h_1 and h_2 are

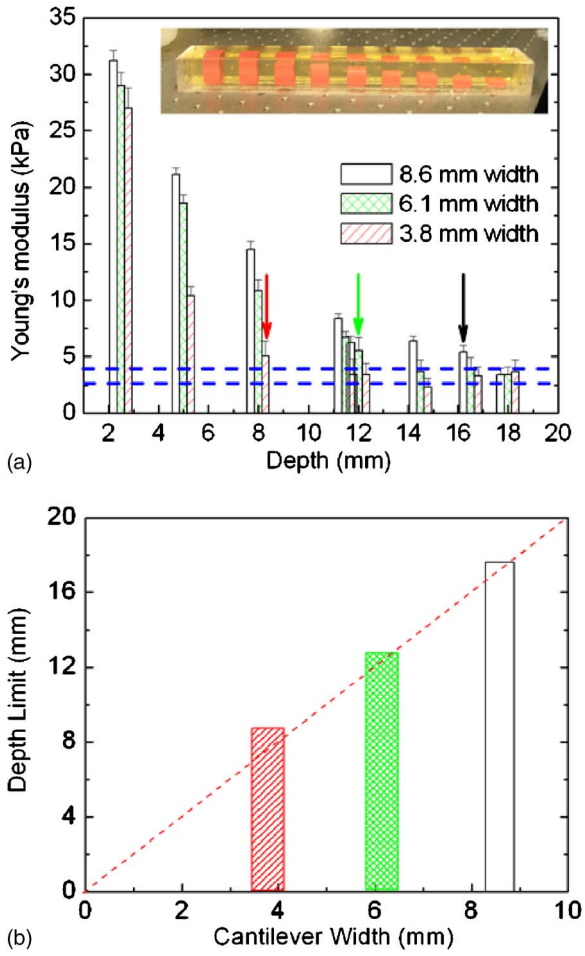

FIG. 5. (Color online) (a) Elastic modulus of modeling clay inclusions embedded at various depths in a gelatin matrix and (b) depth sensitivity limit vs cantilever width. The elastic modulus of the gelatin matrix was 3.8±1 kPa as indicated by the range between the two horizontal dashed lines. The inset in (a) shows the photograph of the nine inclusions of model I.

larger than h_i. If the inclusion is deeper than the depth sensitivities of the cantilevers, then the above analysis is not valid.

III. RESULTS AND DISCUSSIONS

A. Depth sensitivity

To experimentally determine the depth sensitivity of the cantilevers, indentation tests were carried out at the gelatin surface above the centers of the modeling clay inclusions in model I. In Fig. 5(a), we plot the measured elastic moduli of the model tissue above the center of the modeling clay inclusions versus the known depths of the inclusions for cantilevers A (white bars), B (cross-shaded bars), and C (line-shaded bars). Note that in deducing the effective elastic modulus of the model tissues, Poisson's ratio of the inclusion was taken as 0.5, as validated in Ref. 22. As can be seen in Fig. 5(a), the measured effective elastic modulus decreased with an increasing depth and saturated at about 3.8±1 kPa, which was the elastic modulus of the gelatin matrix as shown in Fig. 3(b). The elastic modulus range of the gelatin matrix is marked by the two horizontal dashed lines in Fig. 5(a). We empirically defined a cantilever's depth sensitivity limit as

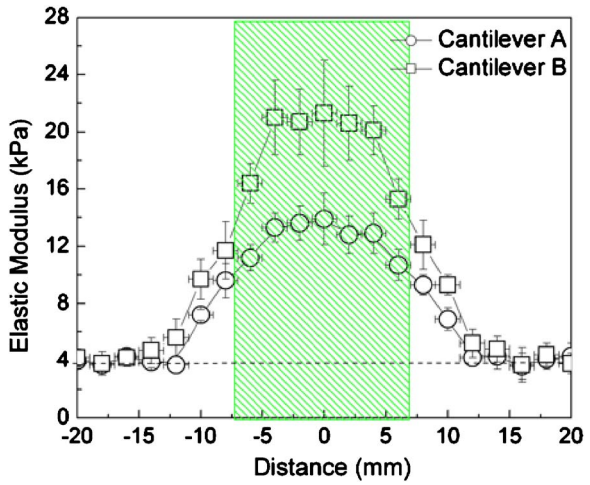

FIG. 6. (Color online) Effective elastic modulus vs the distance from the center of the inclusion obtained with cantilever A (open circles) and cantilever B (open squares).

the largest depth at which the measured effective elastic modulus on the gelatin surface was larger than and experimentally distinguishable from that of the gelatin matrix. With this criterion, we obtained 8, 12, and 17 mm as the depth sensitivity limit for cantilevers A, B, and C, respectively. The dependence of the depth sensitivity limit on the cantilever width (the linear dimension of the indentation area) is summarized in Fig. 5(b), where we plot the depth sensitivity limit versus the cantilever width. As can be seen, the depth sensitivity limit was linear with cantilever width with a slope of about 2, indicating that for a given cantilever, the depth sensitivity limit was about twice its width. Therefore, the results shown in Figs. 5(a) and 5(b) indicate that in an indentation experiment, the depth affected by the indentation was roughly twice the linear dimension of the indentation area. Tissues below the depth sensitivity limit was unaffected by the indentation, thus insensitive to the measurements.

B. Inclusion depth and elastic modulus measurement using two cantilevers

With the depth sensitivity of each cantilever determined above, it is possible to determine the elastic modulus and depth of an unknown inclusion. In model II, we embedded nine inclusions out of three different kinds of modeling clays of various heights. As mentioned above, the elastic moduli of the green, blue, and red modeling clays were independently measured and determined to be 54±12, 92±9, and 145±10 kPa, respectively, using the indentation test as described in Sec II C. The known elastic moduli of the inclusions in model I and model II were also listed in Table II. As an example, we show the effective elastic modulus profiles of inclusion 2 in model II (see Table II), as measured using cantilever A (open circles) and cantilever B (open squares) in Fig. 6. From Fig. 6, one can see that at locations away from the center of the inclusion at $x=0$, the effective moduli measured by cantilever A were essentially the same as those measured by cantilever B. Moreover, the values of the effective elastic moduli at locations away from the inclusion, 4.1±0.4 kPa, matched that of the gelatin matrix independently obtained in Fig. 3(b), 3.8±0.5 kPa, as marked by the

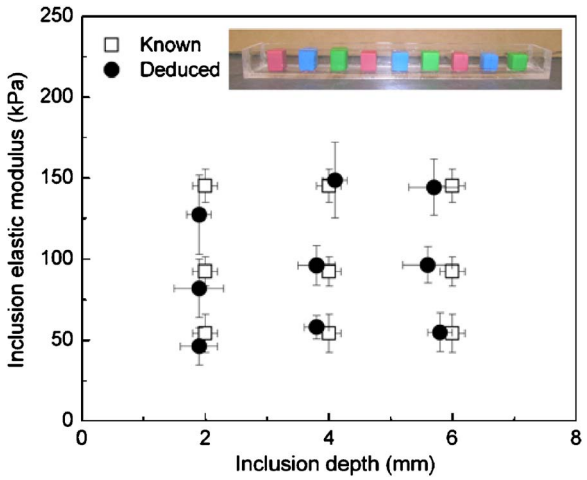

FIG. 7. (Color online) Inclusion elastic modulus vs inclusion depth. Note that for all nine inclusions, the deduced values agree with the known values, indicating that the present approach of using two cantilevers of different widths was indeed capable of determining the inclusion elastic modulus and inclusion depth simultaneously. The inset shows the photograph of the nine inclusions of model II.

horizontal dashed line in Fig. 6. Therefore, in the following analyses, for each of the nine inclusions in model II, two elastic modulus profiles were measured using two different cantilevers, cantilever A and cantilever B, as illustrated in Fig. 6. The elastic modulus of the gelatin matrix was then taken as values at locations away from the inclusion where the elastic moduli measured by the two cantilevers at the same location were the same. The elastic modulus and the depth of the inclusion were then deduced using the elastic modulus values obtained away from the inclusion (e.g., 4.1 ± 0.4 kPa in Fig. 6) as input for the elastic modulus of the gelatin matrix for Eqs. (3) and (4). With $h_1=8$ mm and $h_2=12$ mm for cantilever A and cantilever B, respectively [as the determined from Figs. 5(a) and 5(b) above] and $E_1=14\pm2$ kPa and $E_2=22\pm3$ kPa, respectively (as determined by the peak effective elastic modulus values measured by cantilever A and cantilever B as shown in Fig. 6) as input, Eqs. (3) and (4) were then simultaneously solved for two unknowns, the inclusion depth h_i and the inclusion elastic modulus E_i, using MAPLE 10 (Maplesoft, Ontario, Canada). The deduced $h_i=2\pm0.4$ mm and $E_i=82\pm18$ kPa were consistent with the known depth of 2 ± 0.3 mm and elastic modulus of 92 ± 9 kPa of inclusion 2 of model II, as shown in Table II. In Fig. 7, we summarize the deduced inclusion elastic modulus and inclusion depth in the two-dimensional (2D) elastic versus depth plot. The inset in Fig. 7 shows the photograph of model II which contained the nine inclusions of various moduli and various depths. Also plotted in Fig. 7 are the known values of the inclusion moduli and inclusion depths. As can be seen, for all nine inclusions, the deduced values and the known values were within each other's experimental uncertainty in the 2D elastic modulus versus depth space, indicating that the present approach of using two cantilevers with different widths was indeed capable of determining the inclusion elastic modulus and inclusion depth simultaneously.

It should be noted that for the present method to work, the depth sensitivities of the cantilevers must be sufficiently larger than the depth of the inclusion as discussed above. Therefore, only when both cantilevers produce bell-shaped elastic modulus profiles such as the one shown in Fig. 6, Eqs. (3) and (4) can be used to deduce the inclusion elastic modulus and inclusion depth.

In addition, the inclusion elastic modulus, inclusion depth, and the lateral size of the inclusion, can also be deduced from the effective elastic profiles shown in Fig. 6. From the bell-shaped elastic modulus profile, the lateral size of the inclusion was estimated as the width at half the peak height. The lateral sizes of the inclusion as deduced from Fig. 6 were 16 ± 1 and 15 ± 1 mm as measured by cantilevers A and B, respectively, consistent with the known value of 16 mm. The location of the inclusion was marked by the shaded square in Fig. 6.

ACKNOWLEDGMENTS

This work is supported in part by the National Institutes of Health under Grant No. 1 R01 EB000720.

[1] J. F. Greenleaf, M. Fatemi, and M. Insana, Annu. Rev. Biophys. Biophys. Chem. **5**, 57 (2003).
[2] A. P. Sarvazyan, J. Acoust. Soc. Am. **93**, 2329 (1993).
[3] P. S. Wellman, R. D. Howe, E. Dalton, and K. A. Kern, http://biorobotics.harvard.edu/pubs/mechprops.pdf
[4] G. W. Schmid-Schonbein, K.-L. Paul, H. Tozeren, R. Skalak, and S. Chien, Biophys. J. **36**, 243 (1981).
[5] P. Wakely, W. J. Frable, and J. S. Kneisl, Cancer Cytopathology **93**, 35 (2001).
[6] Y. Murayama and S. Omata, Sens. Actuators, A **109**, 202 (2004).
[7] Y. Murayama, C. E. Constantinou, and S. Omata, Sens. Actuators, A **120**, 543 (2005).
[8] A. Samani, J. Bishop, C. Luginbuhl, and D. B. Plewes, Phys. Med. Biol. **48**, 2183 (2003).
[9] J. W. Klaesner, P. K. Commean, M. K. Hastings, D. Zu, and M. J. Mueller, IEEE Trans. Neural Syst. Rehabil. Eng. **9**, 232 (2001).
[10] J. W. Klaesner, M. K. Hastings, D. Zou, C. Lewis, and M. J. Mueller, Arch. Phys. Med. Rehabil. **83**, 1796 (2002).
[11] K. Rome and P. Webb, Clin. Biomech. (Bristol, Avon) **15**, 298 (2000).
[12] Y. Huang, Y. Zheng, and S. Leung, Clin. Biomech. (Bristol, Avon) **20**, 145 (2005).
[13] L. Han, J. A. Noble, and M. Burcher, Ultrasound Med. Biol. **29**, 813 (2003).
[14] Y. Zheng and A. F. T. Mak, IEEE Trans. Rehabil. Eng. **7**, 257 (1999).
[15] A. Manduca, T. E. Oliphant, M. A. Dresner, J. L. Mahowald, S. A. Kruse, E. Amromin, J. P. Felmlee, J. F. Greenleaf, and R. L. Ehman, Med. Image Anal **5**, 237 (2001).
[16] J. Ophir, I. Cespedes, H. Ponnekanti, Y. Yazdi, and X. Li, Ultrason. Imaging **13**, 111 (1991).
[17] D. B. Plewes, J. Bishop, A. Samani, and J. Sciarretta, Phys. Med. Biol. **45**, 1591 (2000).
[18] R. Sinkus, J. Lorenzen, D. Schrader, M. Lorenzen, M. Dargatz, and D. Holz, Phys. Med. Biol. **45**, 1649 (2000).
[19] A. Markidou, W. Y. Shih, and W.-H. Shih, Rev. Sci. Instrum. **76**, 064302 (2005).
[20] H. O. Yegingil, W. Y. Shih, W. Anjum, A. D. Brooks, and W.-H. Shih, Mater. Res. Soc. Symp. Proc., **898E**, L01 (2006).
[21] S. T. Szewczyk, W. Y. Shih, and W.-H. Shih, Rev. Sci. Instrum. **77**, 044302 (2006).
[22] H. O. Yegingil, W. Y. Shih, and W.-H. Shih, J. Appl. Phys. **101**, 054510 (2007).
[23] G. M. Pharr, W. C. Oliver, and F. R. Brotzen, J. Mater. Res. **7**, 613 (1992).